Chemosphere 259 (2020) 127414

Contents lists available at ScienceDirect

Chemosphere

journal homepage: www.elsevier.com/locate/chemosphere

# The effect of hybrid zinc oxide/graphene oxide (ZnO/GO) nano-catalysts on the photocatalytic degradation of simazine

K. Flores [a], C. Valdes [a], D. Ramirez [a], T.M. Eubanks [a], J. Lopez [b], C. Hernandez [b], M. Alcoutlabi [b], J.G. Parsons [a, *]

[a] Department of Chemistry, University of Texas Rio Grande Valley, 1 W University Blvd., Brownsville, TX, 78521, USA
[b] Department of Mechanical Engineering, University of Texas Rio Grande Valley, 1201 University Dr, Edinburg, TX, 78539, USA

## HIGHLIGHTS

- ZnO/GO hybrid material was successfully synthesized and characterized using XRD, SEM, and XPS.
- The ZnO band gap was observed to shift to approximately 400 nm with the GO support.
- Effective removal of simazine from aqueous solution under visible light was achieved from pH 2 -pH 8.
- Kinetics were determined to follow second order as shown below: $rate = k[SIM]^2[ZnOGO]^0 = k[SIM]^2$.
- The effect of temperature on the rate of simazine degradation was dependent on the amount of ZnO present on the GO.

## ARTICLE INFO

*Article history:*
Received 22 March 2020
Received in revised form
11 June 2020
Accepted 11 June 2020
Available online 22 June 2020

Handling Editor: Shane Snyder

*Keywords:*
Photocatalysis
Zinc oxide
Graphene oxide
Hybrid nanomaterial
Simazine

## ABSTRACT

The photocatalytic degradation of simazine (SIM) was investigated using zinc oxide/graphene oxide (ZnO/GO) composite materials under visible light irradiation. The reaction kinetics was studied to optimize the reaction parameters for efficient degradation of SIM. Batch studies were performed to investigate the effects of initial reaction pH, the loading of the ZnO onto GO, and mass of catalyst on the removal of SIM from aqueous solution. A pH of 2 was determined to be the optimal reaction pH for the different ZnO-loaded GO catalysts. In addition, a mass of 40 mg of catalyst in the reaction was observed to be the most effective for the catalysts synthesized using 20 and 30 mmol of $Zn^{2+}$ ions; whereas a mass of 10 mg was most effective for the ZnO/GO composite material synthesized using 10 mmol $Zn^{2+}$ ions. The reaction was observed to follow a second-order kinetics for the degradation process. Furthermore, the synthesized ZnO/GO composite catalysts resulted in higher reaction rates than those observed for pure ZnO. The 30 mmol ZnO/GO composite expressed a rate of SIM degradation ten times greater than the rate observed for pure ZnO, and sixty-two times greater than the rate of photolysis. In addition, the catalyst cycling exhibited a constant photocatalytic activity for the ZnO/GO composite over three reaction cycles without the need of a conditioning cycle.



## 1. Introduction

The extensive use of herbicides in the environment has led to the accumulation of persistent organic pollutants (POPs) Pollution by herbicide residues, such as the chloro−s−triazine family, has received great attention recently due to their frequent use, ability to distribute into water sources, and their possible carcinogenic effects (EPA, 2006). Simazine (SIM), a widely used chloro-*s*-triazine herbicide, that can disperse effectively in ground water with an almost identical structure to atrazine, another pollutant of major concern (EMBDPR, 2004; Beste, 1983). SIM ingestion has been linked to a variety of health complications, which include disruptions of the central nervous system, DNA replication, metabolism, and normal sexual functions in males (Bányiová et al., 2016; EPA, 1995).

Typical methods for the removal of SIM from water include reverse osmosis, adsorption using activated carbon, ozonation, Fenton oxidation, UV photolysis, and UV $H_2O_2$ oxidation systems (Chu et al., 2009). Activated carbon systems work well for the remediation of organics from water however, these systems tend to

* Corresponding author.
*E-mail address:* jason.parsons@utrgv.edu (J.G. Parsons).

https://doi.org/10.1016/j.chemosphere.2020.127414
0045-6535/

be non-cost effective in upscaling (Arvanitoyannis and Varzakas, 2008). Ozonation, UV systems, and Fenton oxidation systems are non-specific and create secondary contaminants. Therefore, there is a need to develop cost effective and efficient methods to remove triazines from water (Mills et al., 1993).

Photocatalytic degradation may be a feasible method to use for the removal of triazines from water sources. The photocatalytic degradation of POPs has attracted much attention due to its low cost, versatility, effectiveness, and mild reaction conditions (Kabra et al., 2004; Xiao et al., 2020). Photocatalysis works through the generation of reactive oxygen species (ROS) from water, that can react with organic pollutants, hence resulting in the pollutant degradation (Mills and Hunte, 1997). Photocatalysts have the capability of degrading different pollutants from water sources (Kabra et al., 2004). Metal oxide semiconductor materials such as zinc oxide (ZnO), iron oxides ($Fe_xO_y$), and titanium dioxide ($TiO_2$) are considered photocatalytic materials, which have been shown to generate innocuous products and eliminate the generation of secondary waste (Kabra et al., 2004).

Widely studied photocatalysts such as $TiO_2$ and ZnO exhibit large band gaps (3.2 eV), which require UV irradiation to facilitate the photocatalytic process (Lee et al., 2012; Asahi et al., 2001). Until recently, the use of UV sensitized materials was considered an energetically favorable process compared to other remediation methods. More recently, a shift into the use of solar radiation spectrum has occurred as the desirable means of energy to perform photocatalysis (Anpo and Takeuchi, 2003; Wang et al., 2019). Hybrid materials containing $TiO_2$ and ZnO anchored to carbonaceous components have also shown enhanced absorption under solar irradiation (Saud et al., 2015, Chen et al., 2010; Lettmann et al., 2001; Xiao et al., 2020).

Lavand and Malghe have used C/ZnO/Cds in the visible light photocatalytic degradation of chlorophenol (Lavand and Malghe, 2015). The study showed exceptionally high photocatalytic activity with complete degradation of chlorophenol within 150 min of the reaction. A study reported on the use of enhanced catalytic activity for the degradation of atrazine using Cu doped ZnO—$C_3N_4$ showed that a shift into the visible region in absorption was observed. This Cu doped catalyst has shown over 90% removal of atrazine. Similarly, a Ag coated ZnO nanoflowers-based photocatalyst showed increased catalytic activity for the degradation of methylene blue compared with individual Ag and ZnO nanoparticles (NPs) (Shahid et al., 2020). Ebrahimi et al. showed that Mn doped ZnO-graphene nanocomposite was successful in degrading 50—80% of 2,4-dichlorophenoxyacetic acids in aqueous solution (Ebrahimi et al., 2019).

In the present study, a series of hybrid ZnO/GO photocatalysts, with different ZnO:GO ratios, were synthesized and tested for the photocatalytic degradation of SIM as a model for triazine compounds in water. The structure and morphology of the ZnO/GO photocatalysts were characterized using X-ray diffraction (XRD), scanning electron microscopy (SEM) and UV-VIS. Furthermore, studies were conducted to determine the effects of pH, time, and catalyst loading on the degradation of SIM using a 100 W metal halide lamp as the radiation source. Further catalytic studies were performed to determine the efficiency and durability of the photocatalysts over multiple catalytic cycles.

## 2. Materials and methods

### 2.1. Photocatalyst synthesis and characterization

#### 2.1.1. Graphene oxide synthesis

The graphene oxide starting material was synthesized using a modified Hummers' method (Marcano et al., 2010). In brief 3.0 g of graphite flake, 1.5 g of $NaNO_3$, and 69 mL of $H_2SO_4$ were added to a round bottom flask. The mixture was homogenized under magnetic stirring and cooled to 4°C. Subsequent to cooling, 9.0 g of $KMnO_4$ were added in small portions, maintaining the reaction temperature under 20°C. The reaction mixture was heated to approximately 35°C for 30 min followed by a dropwise addition of 138 mL of 18 MΩ $H_2O$ (MW), ensuring the temperature was maintained below 60°C. Subsequent to the addition of water, the reaction mixture was heated to 98°C and held at this temperature for 15 min, then cooled back to room temperature. After cooling, the reaction was combined with 420 mL of MW and 3 mL of 30% $H_2O_2$. The GO particles were collected using vacuum filtration, washed with MW followed by acetone, and then dried overnight at 85°C.

#### 2.1.2. ZnO/GO photocatalyst synthesis

In a typical synthesis, 1.0 g of GO was added to a 1.0 L flask followed by the addition of 500 mL of $Zn(NO_3)_2$ $6H_2O$ at a specific concentration. The catalysts were synthesized using different $Zn(NO_3)_2$ $6H_2O$ concentrations of 30, 20, and 10 mM. These mixtures were titrated with 1 M NaOH to give a 2:1 M ratio of $OH^-$:$Zn^{2+}$. The titrated GO/Zn suspensions were heated to 60°C, for 2 h and cooled to room temperature. The ZnO/GO particles were filtered using vacuum filtration, washed using MW followed by acetone, and dried overnight at 85°C.

#### 2.1.3. X-ray diffraction (XRD)

XRD analysis was performed using a Bruker D2 Phaser Diffractometer.

The diffraction data were collected using a Co source $K_\alpha$ 1.789 Å and a Fe-filter. The data were collected from 5—80° in 2θ, using a step size of 0.05° and a counting time of 2 s per step. The data analysis was performed using the Le Bail fitting procedure in the Fullprof software and existing crystallographic data from literature (LeBail et al., 1988; Carvajal, 1993; Howe et al., 2003).

#### 2.1.4. Scanning electron microscopy (SEM)

Scanning electron microscopy (SEM) images were collected using a Zeiss EVO LS 10 scanning electron microscope.

Electron micrographs were collected at working distances ranging from 6.0 to 6.5 mm with an accelerating voltage ranging from 10.75 to 20.71 KeV.

#### 2.1.5. UV-VIS spectroscopy

Band Gap measurements were performed on a PerkinElmer Lambda 950 equipped with a 150 mm integrating sphere.

The samples were pressed into pellets and suspended in the integrating sphere. The data were recorded in reflectance mode from 200 to 600 nm. The calculation of the Band Gap for the materials was performed using the Kubelka-Munk method (López and Gómez, 2012).

#### 2.1.6. X-ray photoelectron spectroscopy

XPS analysis was performed on the materials using a Thermo Scientific K-α spectrometer equipped with an A1 source ($K_\alpha$ E = 1.487 keV) with a 400 μm spot size.

### 2.2. Photocatalytic studies

#### 2.2.1. pH study

A mass of 40 mg of photocatalyst was combined with 4 mL of a 25-ppm pH adjusted SIM solution.

The pH adjustment of the SIM solutions was performed using either dilute hydrochloric acid or dilute sodium hydroxide. The reaction solutions were placed in the New Brunswick Scientific

Innova 44 incubator at 20 °C. Both reaction and control samples were equilibrated under irradiation from a 100 W metal halide lamp for 1 h. The control samples consisted of SIM in the absence of any photocatalyst. The reaction and control samples were repeated in triplicate for statistical purposes. The samples were centrifuged and the supernatant was analyzed using HPLC.

#### 2.2.2. Catalyst loading

Loading masses of 10, 20, 40, 60, and 80 mg were added to the SIM solutions at the optimum reaction pH as previously determined (pH 2).

The specified mass of photocatalyst was combined with 4 mL of a 25-ppm pH adjusted SIM solution. Triplicates of both the reaction and control samples were placed in the Innova 44 incubator with a controlled reaction temperature of 20 °C. The reaction and control samples were equilibrated under illumination for 1 h. Subsequent to reaction, the samples were centrifuged, the supernatants extracted, and analyzed using HPLC.

#### 2.2.3. Kinetics studies

A mass of 40 mg of catalyst was added to 4 mL of a 25 ppm SIM solution adjusted to the optimum reaction pH 2.

At 15-min intervals, 150 μL samples were extracted from both the reactions and control solutions over a 2-hr reaction period. The extracted samples were centrifuged while the supernatant was analyzed using HPLC for SIM concentrations. The reaction and control samples were performed in triplicate for statistical purposes. The kinetic studies were performed at different temperatures of 11, 22 and 30 °C. The kinetic studies were used to determine the activation energy of the photocatalytic degradation of SIM.

#### 2.2.4. Concentration variation

The reactions were performed using SIM with different concentrations of 25, 12.5, and 6.25 ppm and with optimal reaction conditions of pH and loading mass, as were determined from earlier studies. 40-mg mass of the photocatalyst was weighed placed in 4 mL of a 25 ppm SIM solution at pH 2.0. The reaction was performed in an Innova 44 incubator at a controlled temperature 20 °C. Under a constant irradiation, both reaction and control samples were equilibrated at 15-min time intervals 150 μL samples were extracted from both the sample and control reaction mixtures. The samples were then centrifuged to extract the supernatants for analysis using HPLC.

#### 2.2.5. Catalytic cycling studies

A mass of 1.5 g of catalyst and 150 mL of 25 ppm SIM solution were placed in the Innova 44 incubator at a controlled temperature of 20 °C with constant stirring. Both reaction and control samples were equilibrated under illumination for 1 h under irradiation using a 100 W metal halide lamp. The samples were then centrifuged, and the supernatant was collected for analysis using HPLC. The procedure was repeated two more times for a total of three reaction cycles.

#### 2.2.6. High-performance liquid chromatography (HPLC)

A Thermo Scientific Ultimate 3000 HPLC equipped with reverse phase C-18 column and UV−Vis detector was used to measure the SIM concentrations.

The mobile phase was a 35:65 mixture of acetonitrile and ammonium acetate buffer (0.1 M, pH6). The HPLC analysis for all control reaction and samples consisted of a 10 μL injection, with a 1 mL/min flow rate, a column temperature of 30 °C, and a wavelength of 225 nm. The total run time per injection was of 10 min. The experiments were performed in triplicate for statistical purposes.

## 3. Results and discussion

### 3.1. XRD results

Figure S1 shows the diffraction pattern and the Le Bail fitting for the starting GO material. Table S1 shows the determined lattice parameters, and goodness of the fit ($\chi^2$) of the Le Bail fitting for the synthesized graphene oxide, ZnO and the ZnO/GO hybrid photocatalysts, Fig. 1 shows the diffraction patterns and Le Bail fittings for the synthesized ZnO/GO and ZnO materials. The crystal structure of the ZnO/GO samples was determined through comparison of their XRD analysis to existing crystallographic data from literature. (Howe et al., 2003; López and Gómez, 2012; Krishnamoorth et al., 2013). The crystal structure of the ZnO/GO composites, and pure ZnO, was determined to be in the $P6_3MC$ space group, which corresponds to the hexagonal (wurtzite) crystal lattice of ZnO (Yu and Yu, 2008). In addition, the graphene oxide sample was also observed to maintain a hexagonal crystal lattice with the $P6_3MC$ space group (Howe et al., 2003; Krishnamoorth et al., 2013).

The first peak of the ZnO/GO composites appeared at approximately 12°, in $2\theta$, corresponding to the reflection for the (001) plane of graphene oxide. The peak at $2\theta = 12°$ was most apparent for the 10 mmol ZnO/GO composite photocatalyst and was less visible in the 20 & 30 mmol ZnO/GO composites (Fig. 1A−C). The subsequent peaks observed for all ZnO/GO composites, were located at 37°, 40°, and 42.5° with relatively high intensities, corresponding to ZnO diffraction peaks. These diffraction peaks correspond to the (100), (002), (101) reflections for the ZnO planes. The final three peaks, located at 56°,67°, and 75° also correspond to the ZnO material, which are the (110), (200), and (103) planes. The diffraction pattern for the pure ZnO material is shown in Fig. 1D.

### 3.2. XPS analysis

Figure S2 shows the XPS survey spectrum for the ZnO/GO photocatalysts. The results in Fig. S2 confirm the presence of zinc, oxygen, and carbon elements in the ZnO/GO photocatalysts. The electrons from core level Zn 2p 1/2 and 3/2 binding were expressed at energies of 1047 and 1024 eV (Stathi et al., 2015). The peaks observed at 534 eV & 287 eV correspond to the electron shells of O 1s and C 1s (Atchudan et al., 2016). All photocatalysts synthesized in this work contained the same three elements Zn, O and C. The 30 mmol ZnO/GO photocatalyst was comprised of 63.66% zinc, 11.84% oxygen, and 24.50% carbon. Measurements for the 20 mmol ZnO/GO catalyst expressed 54.82% zinc, 15.47% oxygen, and 29.71% carbon presence; while the 10 mmol ZnO/GO catalyst was comprised of 42.21% zinc, 19.75% carbon, and 38.04% carbon (Table S2). Fig. S3, shows the XPS for the Zn 2P, C 1S, and O 1S, of the 10 mM ZnO-GO hybrid material freshly synthesized. Fig. S4 shows the XPS data for the 10 mM ZnO-GO hybrid material after use in one catalytic cycle. The Zn 2P spectrum shows the presence of the Zn−O−C=O binding by the presence of the 1023.6 eV peak in the fitting as well as the presence of Zn−O 1022.3 eV (Lloyd et al., 2015; Tien et al., 2013; Zhang et al., 2015; Ward and Weber, 1968). The XPS results also indicated trace amounts of Zn−OH (peak located at 1023.1 eV) in the freshly synthesized ZnO/GO materials. The Zn−OH was removed after one catalytic cycle. The O 1S spectrum shows the presence of C−O (533 eV) interaction and O−Zn (530.8 eV) interactions. After the reaction was proceeded, only the C−O and Zn−O bonds were visible in the XPS spectrum for the O 1S of Fig. S4.

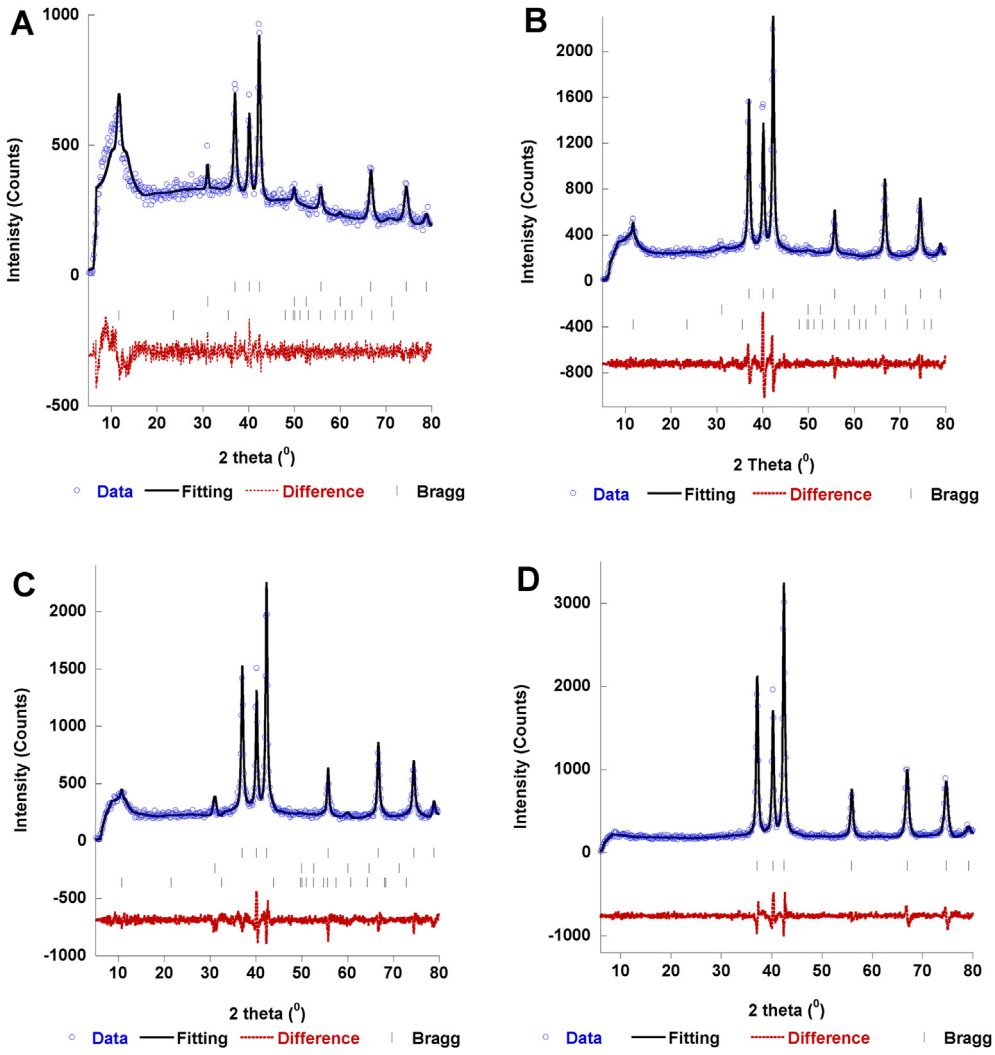


**Fig. 1.** Le Bail fitting of the collected X-ray diffraction for the synthesized ZnO-GO hybrid material **A.)** synthesized using 10 mM $Zn(NO_3)_2$, **B.)** synthesized using 20 mM $Zn(NO_3)_2$, **C.)** synthesized using 30 mM $Zn(NO_3)_2$, and **D.)** ZnO particles. (note: lowest Bragg peak indicators are for an expanded graphite from the graphene oxide synthesis, middle Bragg peak indicators are for graphite, and top Bragg Peak indicators are for ZnO).

The C 1S spectrum for both the before and after reaction samples shows a mixture of C–O (288.7 eV), Metal—O-C-O (285.9 eV) bonding, and C–C (284.9 eV) bonding presence indicating the presence of GO bound to Zn (Tien et al., 2013; Zhang et al., 2015; Ward and Weber, 1968). Figs. S5–S8 show the freshly synthesized ZnO/GO composite materials before and after reaction for the 20- and 30-mM synthesis. The formation of Zn–O–H in the ZnO/GO composite is not observed in the products, which may be due to the concentration of the compounds present in the samples. The XPS results for the ZnO/GO hybrid materials show similarity in the surface structure before and after the degradation reactions, which indicates a chemical stability of the photocatalyst. The XPS results also indicate the successful synthesis of the ZnO/GO hybrid materials by the observation of the Zn–O–C=O in the XPS data. Table S2 shows the calculated percentages of elements in the ZnO/GO hybrid material after synthesis, which shows an increase in the amount of Zn present in the samples, with increased Zn concentration in the synthesis.

### 3.3. Results from the band gap study

The results of the band gap studies (Table S3) show that the addition of GO to the ZnO resulted in a decreased band gap of the ZnO/GO composite. In fact, the band gap shifts towards the visible region. It is known that ZnO has a band gap in the UV which starts at 367 nm, however the 10 mM ZnO-GO composite band gap was 378 nm, the band gap for the 20 mM ZnO/GO composite was determined to be at 399 nm while for the 30 mM ZnO/GO composite, the band was determined to be at 381 nm. The decrease in the absorption wavelength observed at the 30 mM can be explained through the material's optical behavior moving towards "pure" ZnO and away from the composite.

### 3.4. SEM results

Figure S9A shows the SEM image of the 10 mmol ZnO/GO composite where the white cluster correspond to the zinc oxide platelets attached to a graphene oxide. Fig. S9 B shows the SEM image of the 20 mmol ZnO/GO composite, which shows a higher concentration of zinc oxide clusters with less exposed graphene oxide compared to the 10 mmol material. Fig. S9C shows the SEM image of the 30 mmol ZnO/GO composite which shows the highest amount of zinc oxide clusters and the lowest amount of exposed graphene oxide. The results confirm that the ZnO is deposited onto

the surface of the GO material.

### 3.5. Initial pH results

Fig. 2 shows the photocatalytic degradation results of the SIM in the synthesized ZnO/GO composites (30, 20, 10 mmol) and pure ZnO that were tested over a pH range from 2 through 8. The synthesized materials showed the highest catalytic activities at a pH of 2. The results showed 1.965 mg/g of SIM was degraded by the 10 mmol ZnO/GO composite, 2.434 mg/g of SIM was degraded by 20 mmol of the composite, 2.049 mg/g of SIM was degraded by the 30 mmol of composite, and 1.347 mg/g of SIM was degraded by the pure ZnO photocatalyst material. The photocatalytic degradation of the SIM, observed with the composite materials, showed a decrease from pH 2 to 5 (0.578 mg/g), and an increase from pH 5–6 while the reaction plateaued (reached a constant value of SIM removal of approximately 1.6 mg/g) at pH 6 remained constant to pH 8. Pure ZnO, showed a decrease in photocatalytic activity from pH 3 to pH 7 (0.168 mg/g), however, an increase in degradation at pH 8 (0.573 mg/g) was observed. Ward and Weber observed a trend between pH and SIM solubility (Ward and Weber, 1968). From a pH of 2–3, the solubility of SIM was observed to decrease from 0.78 × 10-4 M to 0.29 × 10-4 M. However, the maximum solubility for SIM was observed at a pH of 1 (5.81 × 10-4) and decreased thereafter as the solution became more basic. The solubility mechanism is dependent on the protonation of the nitrogen atoms, locked in the ring structure, at positions ortho to the chlorine substituent (Ward and Weber, 1968). In a recent study by Yang et al., the degradation of orange II dye by Fe on $Fe_3O_4$ was shown to be pH dependent with the highest degradation observed around pH 3, which showed 99% removal within 5 min (Yang et al., 2020). A study by Xu et al. on the degradation of atrazine showed that the $Fe_3O_4$-Sepiolite catalysis and persulfate increased the degradation of atrazine at low pH (Xu et al., 2019). The authors suggested that the enhanced degradation at lower pHs may have occurred for two reasons: a) increased activity of active sites on the catalysts surface and b) increased generation of ROS species by persulfate (Xu et al., 2019). The degradation of chlorophenols with nanoscale zerovalent iron has also been shown to be highly catalytic at acidic pHs. Bao et al. showed the degradation of chlorophenol was effective using nanosized zero valent iron particles under acidic conditions but it was ineffective at basic pHs due to the inability to produce hydroxyl radicals (Bao et al., 2019).

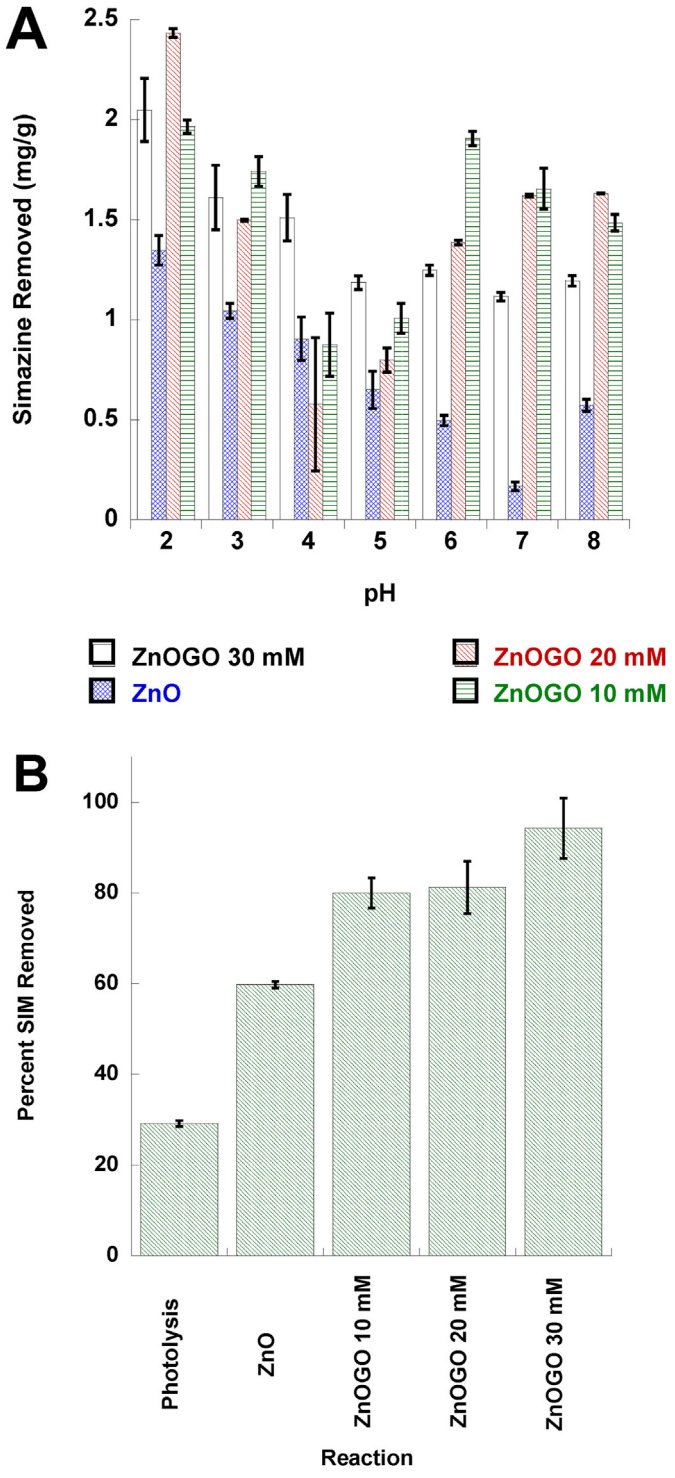


**Fig. 2. A.)** Effect of pH on the simazine removal from solution using ZnO/GO hybrid material and ZnO nanomaterial. **B.)** Percent removal of simazine from aqueous solution at pH 2 using photolysis and the various synthesized ZnO and ZnO/GO photocatalysts.

### 3.6. Catalyst loading results

The effect of catalyst loading in the reaction mixture from 10 to 80 mg is shown in Fig. 3. The 20 & 30 mmol ZnO/GO composites, and pure ZnO, showed a similar trend in the percent of SIM degraded and mass of the used photocatalyst. Varying the loading mass from 10 to 40 mg increased the SIM degradation from 64 to 94% for the 20 mmol composite, 55–92% for the 30 mmol composite, and 61–68% for the pure ZnO. Increasing the catalyst loading from 40 to 80 mg showed no change in the percentage of degraded SIM. The plateau observed in the photocatalytic degradation, associated with higher loading masses, can be attributed to an increase in opacity in the solution (Chu et al., 2009). A loading of 40 mg was chosen as optimal for 20 and 30 mmol ZnO/GO composites as well as pure ZnO. The 10 mmol ZnO/GO composite showed different behavior for the percent SIM degradation and catalyst loading mass. Increasing the catalyst mass from 10 to 20 mg resulted in a small decrease in the percentage of SIM degraded; from 20 to 80 mg, the percentage SIM degradation was observed to increase to approximately 83%. Thus, a catalyst loading mass of 10 mg was optimal for the 10 mmol ZnO/GO composite.

### 3.7. Kinetics results

The kinetics were found to be linear only when plotting 1/[SIM] versus time indicating the reaction follows second order kinetics. Table 1 shows the kinetics data and correlation coefficients ($R^2$) for the kinetics plots are for the most part 0.99 or better for the

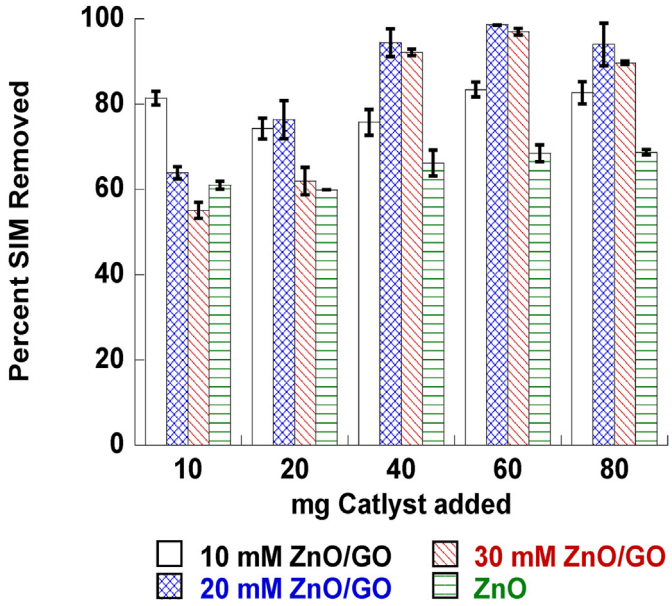


**Fig. 3.** Effect of mass of catalyst added to reaction mixtures at 20 C on the degradation of SIM in aqueous solution.

**Table 1**
Summary of the results from the kinetics studies of the ZnO/GO, pure ZnO, and the non-catalyzed degradation of SIM in aqueous solution determined using 25-ppm concentration of SIM.

| Sample | Temperature (°C) | Slope | $R^2$ |
|---|---|---|---|
| ZnO | 11.5 | $3.1 \times 10^{-3}$ | 0.99 |
| | 20.0 | $4.18 \times 10^{-3}$ | 0.99 |
| | 30.0 | $4.77 \times 10^{-3}$ | 0.98 |
| 10 mM ZnO/GO | 11.5 | $1.06 \times 10^{-2}$ | 1.00 |
| | 20.0 | $6.7 \times 10^{-3}$ | 0.97 |
| | 30.0 | $4.5 \times 10^{-3}$ | 0.99 |
| 20 mM ZnO/GO | 11.5 | $1.05 \times 10^{-2}$ | 1.00 |
| | 20.0 | $9.5 \times 10^{-3}$ | 1.00 |
| | 30.0 | $8.4 \times 10^{-3}$ | 0.99 |
| 30 mM ZnO/GO | 11.5 | $3.68 \times 10^{-2}$ | 1.00 |
| | 20.0 | $4.9 \times 10^{-2}$ | 1.00 |
| | 30.0 | $8.4 \times 10^{-2}$ | 0.98 |
| Photolysis | 11.5 | $1.1 \times 10^{-3}$ | 0.96 |
| | 20.0 | $7.8 \times 10^{-4}$ | 0.94 |
| | 30.0 | $7.1 \times 10^{-4}$ | 0.93 |

catalyzed reactions. The uncatalyzed reactions $R^2$ values were approximately 0.95, indicating less agreement with second order kinetics.

The rate constant found for the 30 mmol ZnO/GO composite was of the largest at $4.9 \times 10^{-2}$ L $mol^{-1} \cdot s^{-1}$), followed by the 20 mmol composite ($9.5 \times 10^{-3}$ L $mol^{-1} \cdot s^{-1}$), 10 mmol composite ($6.7 \times 10^{-3}$ L $mol^{-1} \cdot s^{-1}$), pure ZnO ($4.18 \times 10^{-3}$ L $mol^{-1} \cdot s^{-1}$), and finally direct photolysis ($7.8 \times 10^{-4}$ L $mol^{-1} \cdot s^{-1}$), as shown in Table 1. The reaction rates for all ZnO/GO composite samples surpass the degradation rate expressed by the pure ZnO catalyst, as well as direct photolysis. The 30 mM ZnO/GO composite shows an increase in the rate constant by a factor of approximately 10 compared to the pure ZnO catalyst. Results expressed in Fig. 2B corroborate this enhanced SIM degradation ability by the hybrid nanocatalyst in terms of percent SIM removed per hour of reaction time. The percent removal for the hybrid composites nearly triples the percentage of SIM removed by direct photolysis, and clearly surpass what was reported for the ZnO photocatalyst. The higher rates of degradation, shown by the composite materials in comparison to pure ZnO, may be attributed to the narrowing of the band gap (Table S3), resulting in increased electron mobility. Similar effects have been reported in the literature for materials consisting of semiconductor particles anchored on carbonaceous materials (Sun and Wang, 2014; Pastrana-Martínez et al., 2012; Zheng et al., 2012).

Further studies into the reaction between SIM and ZnO and the ZnO/GO indicate a second order reaction. The change in the SIM concentration with the 30 mM ZnO/GO photocatalyst showed a direct relationship between decreasing the SIM concentration and the decrease in the rate constant (Table S4). As the concentration of the SIM was decreased from 25 ppm to 12.5 ppm, and from 12.5 ppm to 6.25 ppm, the rate of the reaction was observed to decrease by approximately a factor of 4 with each halving of the SIM concentration. The results indicate that the reaction is second order or pseudo-second order with respect to the concentration of SIM in solution. The results of the reactions, using varying amounts of ZnO, are presented in Table S5. The results show that, as the amount of ZnO in the ZnO/GO composite material was decreased, the instantaneous rate constant was not affected. This result indicates that the reaction is zeroth order with respect to the catalysts. Thus, the rate expression can be written as follows

$$rate = k[SIM]^2[ZnOGO]^0 = k[SIM]^2$$

Second order or pseudo-second order kinetics are common in both catalytic and photocatalytic processes (Kim et al., 2008; Daneshvar et al., 2006; Hsieh et al., 2009). The zeroth order with respect to the catalyst indicated the material is only responsible for ROS generation in solution. The results indicate that sufficient catalysts are present to generate ROS species in solution thus the dependence of the reaction order was observed only on the SIM concertation.

### 3.8. Activation energy studies

Table 2 shows the experimentally determined activation energies for the degradation of SIM using various catalysts. Some of the catalyzed reactions showed negative activation energies. The observation of negative activation energies in reactions has been reported in the literature (Mozurkewich and Benson, 1984; Turro et al., 1982; Mills and Davies, 1995). In photocatalysis, negative activation energies have been observed in the photooxidation of 4-chlorophenol using-$TiO_2$-$O_2$ photosystem. The authors showed under reagent limiting conditions ($O_2$) the photooxidation of 4-chlorophenol the activation energies were observed to be negative (Mills and Davies, 1995). In the present study, SIM degradation by the 20 & 10 mmol ZnO/GO catalyst, as well as direct photolysis showed negative activation energies. This may be an effect of the stability and concentration of the generated ROS species, which may have decreased with increasing temperature. A decrease in the stability concentration of ROS species would lead to reduction in reactant concentration and negative activation energy as observed in the photooxidation of 4-chlorophenol (Mills and Davies, 1995).

**Table 2**
Calculated activation energies for the various ZnO/GO, ZnO, and uncatalyzed photochemical degradation of SIM in solution.

| Photocatalyst | Activation Energy (kJ/mol) |
|---|---|
| 30 mmol ZnO/GO | 34.054 |
| 20 mmol ZnO/GO | −8.915 |
| 10 mmol ZnO/GO | −32.275 |
| ZnO | 8.882 |
| Photolysis | −22.028 |

However, the 30 mmol ZnO/GO composite, and pure ZnO catalyst showed positive activation energies. The change in the activation energies, from positive to negative observed with increasing ZnO content, might indicate that ZnO is directly the limiting reagent or indirectly limiting the generation of ROS species. The activation energies for SIM degradation by the various ZnO/GO composite were calculated to be 34.054 kJ/mol for the 30 mmol composite, −8.915 kJ/mol for the 20 mmol composite, and −32.275 kJ/mol for the 10 mmol composite. A trend between the activation energies and amount of zinc oxide present in the catalyst shows increasing the amount of ZnO on GO leads to a more positive activation energy. The positive correlation between activation energy for the ZnO/GO may be indicating a competition between SIM and GO for the generated ROS species. It may be possible that ROS species are reacting with the exposed GO in the photocatalysts. As was noted earlier, lower concentrations of ZnO (10 and 20 mmol) showed higher amounts of exposed GO. Results from the literature indicate that hydroxyl radicals are the primary ROS species for organic compounds degradation and tend to be non-specific in reactions (Gligorovski et al., 2015; Huang et al., 2019). In fact the increase in the reaction temperature promotes more particle-particle interactions; therefore the 10 and 20 mmol composites suffer from higher ROS-GO-ZnO interaction for reasons of proximity, at elevated temperature, which may result in reduced catalytic rates (Strom and Sasic, 2015).

### 3.9. Photocatalytic cycling studies

Fig. 4 shows the removal of SIM from aqueous solution using the different synthesized catalysts for three repeated cycles. The 10 and 20 mmol ZnO/GO composites show a slight increase in the average degradation of SIM over the three cycles. The 10 mmol composite showed a small increase of approximately 10% SIM degradation. The 20 mmol and 30 mmol catalysts remained constant around 80% catalytic degradation in each cycle. The results show the pure ZnO photocatalyst increased from 4.631% SIM degradation during the first cycle and to 47% in the second and third cycles. Large increases in catalytic activity of conversion generally indicate the necessity for a conditioning cycle. The catalysts' residuals were examined using powder XRD analysis. The X-ray diffraction patterns collected for the samples before and after the catalytic cycles do not show a significant change in structure. The diffraction peaks located 37°, 40°, and 42.5° in $2\theta$; corresponding to the reflections of the 100, 002, and 101 planes of zinc oxide, were unchanged, as can be seen in Figs. S10–S13 in the supplemental material for all the synthesized catalytic systems. The increased photocatalytic efficiency, for heterogeneous photocatalysts material, has been attributed to the decrease in particle size (Sorathiya et al., 2016). The particle sizes calculated from the XRD data are shown in Table S6 for the ZnO and ZnO/GO composite materials. There was no appreciable change in the particle size for any of the photocatalytic materials before or after each of the three reaction cycles. The stability of the particle size after reaction indicates that the material is stable while the change in catalytic rate, observed for the pure ZnO photocatalyst, might be due to a change in the surface chemistry.

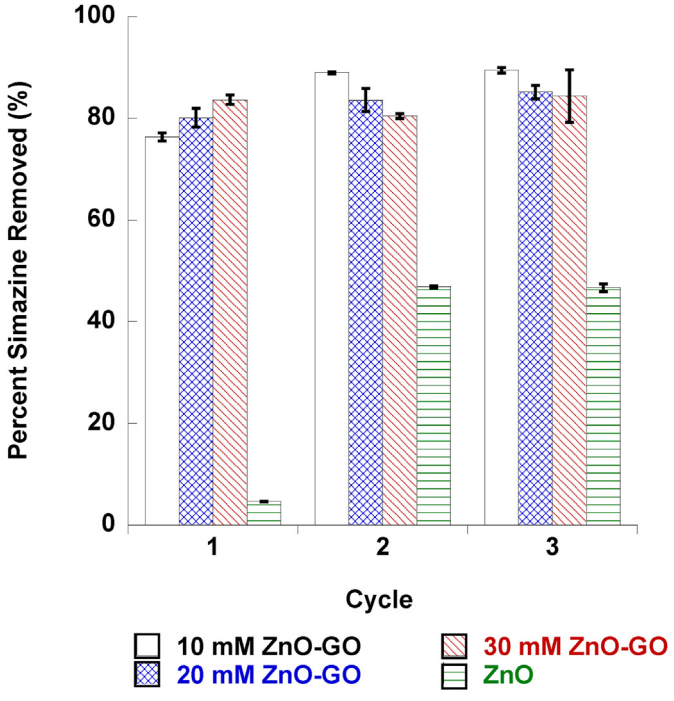


**Fig. 4.** Result of cycling studies for the 10 mM, 20 mM, 30 mM, ZnO/GO, and ZnO synthesized catalysts for the removal of simazine from aqueous solution.

## 4. Conclusions

The as-synthesized ZnO/GO composites (30, 20, 10 mmol Zn on GO) expressed enhanced photocatalytic degradation of simazine under visible light irradiation, as compared to the pure ZnO photocatalyst. The 30 mmol composite showed the greatest rate of SIM degradation, at approximately ten times greater than the rate of pure ZnO, and sixty-two times greater than the rate of photolysis. The as-synthesized composite materials in the present study (work) demonstrated constant photocatalytic degradation of SIM over three catalytic cycles, while pure ZnO required a conditioning cycle before appreciable degradation was observed.

## CRediT authorship contribution statement

**K. Flores:** Data curation, Formal analysis, Writing - original draft, Investigation. **C. Valdes:** Data curation, Writing - original draft, Formal analysis, Investigation. **D. Ramirez:** Data curation, Writing - original draft, Formal analysis, Investigation. **T.M. Eubanks:** Data curation, Investigation. **J. Lopez:** Data curation. **C. Hernandez:** Data curation. **M. Alcoutlabi:** Writing - review & editing, Data curation. **J.G. Parsons:** Project administration, Conceptualization, Writing - original draft, Formal analysis, Funding acquisition, Investigation, Methodology, Resources, Supervision, Validation, Visualization, Writing - review & editing.

## Declaration of competing interest

The authors declare that they have no known competing financial interests or personal relationships that could have appeared to influence the work reported in this paper.

## Acknowledgments

The Department of Chemistry at the University of Texas Rio Grande Valley is grateful for the generous support provided by a Departmental Grant from the Robert A. Welch Foundation (Grant No. BX-0048). M. Alcoutlabi acknowledges support from NSF PREM (DMR-1523577): UTRGV-UMN Partnership for Fostering Innovation by Bridging Excellence in Research and Student Success.

## Appendix A. Supplementary data

Supplementary data to this article can be found online at https://doi.org/10.1016/j.chemosphere.2020.127414.

## References


Anpo, Masakazu, Takeuchi, Masato, 2003. J. Catal. 505–516.
Arvanitoyannis, Ioannis S., Varzakas, Theodoros H., 2008. Food Sci. Technol. 569–628.
Asahi, R., Morikawa, T., Ohwaki, T., Aoki, K., Taga, Y., 2001. Science 269–271.
Atchudan, R., Edison, T.N.J.I., Perumal, S., Karthikeyan, D., Lee, Y.R., 2016 Sep. J. Photochem. Photobiol. B Biol. 162, 500–510.
Saud, Prem Singh, Pant, Bishweshwar, Alam, Al-Mahmnur, Ghouri, Zafar Khan, Park, Mira, Kim, Hak-Yong, 2015. Ceram. Int. 11953–11959.
Bányiová, Katarína, Nečasová, Anežka, Kohoutek, Jiří, Justan, Ivan, Čupr, Pavel, 2016. Chemosphere 145, 148–156.
Bao, Teng, Jin, Jie, Damtie, M.M., Wu, Ke, Yu, Zhi Ming, Wang, Lie, Chen, Jun, Zhang, Yong, Frost, Ray L., 2019. Journal of Saudi Chemical Society 23, 864–878.
Beste, C.E., 1983. Herbicide Handbook of the Weed Science Society of America. Committee, WSSA: Champaign IL.
Carvajal, J.R., 1993. Physica B 192, 55–69.
Chen, Chao, Cai, Weimin, Long, Mingce, Zhou, Baoxue, Wu, Yahui, Wu, Deyong, Feng, Yujie, 2010. ACS Nano 6425–6432.
Chu, Wei, Rao, Yongfang, Hui, W.Y., 2009. J. Agric. Food Chem. 6944–6949.
Daneshvar, N., Salari, D., Niaei, A., Khataee, A.R., 2006. Journal of Environmental Science and Health, Part B. 41 (8), 1273–1290. https://doi.org/10.1080/03601230600962302.
Ebrahimi, Roya, Mohammadi, Mahnaz, Maleki, Afshin, Jafari, Ali, Shahmoradi, Behzad, Rezaee, Reza, Safari, Mahdi, Daraei, Hiua, Giahi, Omid, Yetilmezsoy, Kaan, Shivaraju, H.P., 2019. J. Inorg. Organomet. Polym. Mater. 923–934.
EMBDPR, 2004. Enviromental Fate of Simazine. Enviromental Monitoring Branch Department of Pesticide Regulation: Sacramento, CA. https://pdfs.semanticscholar.org/cc36/03bd48d5b02086a24eb8864aa4e2c56e6371.pdf.
EPA, 1995. Regulations, National Primary Drinking Water Simazine Factsheet. Enviromental Protection Agency, Washington, D.C.. https://nepis.epa.gov/Exe/ZyPDF.cgi/91022ZHL.PDF?Dockey=91022ZHL.PDF
EPA, 2006. Reregistration Eligibility Decision (RED) Document for Simazine. Enviromental Protection Agency, Washington, D.C.. https://archive.epa.gov/pesticides/reregistration/web/pdf/simazine_red.pdf
Gligorovski, Sasho, Strekowski, Rafael, Barbati, Stephen, Vione, David, 2015. Chem. Rev. 115 (24), 13051–13092.
Howe, J.Y., Rawn, C.J., Jones, L.E., Ow, H., 2003. Powder Diffr. 18 (2), 150–154. https://doi.org/10.1154/1.1536926.
Hsieh, Chien-Te, Fan, Wen-Syuan, Chen, Wei-Yu, Lin, Jia-Yi, 2009. Separ. Purif. Technol. 67, 312–318.
Huang, Xiaopeng, Chen, Ying, Walter, Eric, Zong, Meirong, Wang, Yang, Zhang, Xin, Qafoku, Odeta, Wang, Zheming, Rosso, Kevin M., 2019. Environ. Sci. Technol. 53 (17), 10197–10207.
Kabra, Kativa, Chaudhary, Rubina, Sawhney, Rameshwar L., 2004. Ind. Eng. Chem. Res. 7683–7696.
Kim, Seoung-Hyun, Ngo, Huu Hao, Shon, H.K., Vigneswaran, S., 2008. Separ. Purif. Technol. 58, 335–342.
Krishnamoorth, Karthikeyan, Veerapandian, Murugan, Yun, Kyusik, Kim, S., 2013. J. Carbon 53, 38–49.
Lavand, Atul B., Malghe, Yuvraj S., 2015. Journal of Saudi Chemical Society 19, 471–478. https://doi.org/10.1016/j.jscs.2015.07.001.
LeBail, A., Duroy, H., Fourquet, J.L., 1988. Mater. Res. Bull. 23, 447–452.
Lee, Joon Seok, You, Kyeong Hwan, Park, Chan Beum, 2012. Adv. Mater. 1084–1088.
Lettmann, Christian, Hildenbrand, Knut, Kisch, Horst, Macyk, W., Maier, Wilhelm F., 2001. Appl. Catal. B Environ. 215–227.
Lloyd, J.S., Fung, C.M., Alvim, E.J., Deganello, D., Teng, K.S., 2015. Nanotechnology 26, 265303.
López, Rosendo, Gómez, Ricardo, 2012. J. Sol. Gel Sci. Technol. 61, 1–7.
Marcano, D.C., Kosynkin, D.V., Berlin, J.M., Sinitskii, A., Sun, Z., Slesarev, A., Alemany, L.B., Lu, W., Tour, J.M., 2010. ACS Nano 4 (8), 4806–4814.
Mills, Andrew, Davies, Richard, 1995. J. Photochem. Photobiol. Chem. 85, 173–178.
Mills, Andrew, Hunte, Stephen Le, 1997. J. Photochem. Photobiol. Chem. 1–35.
Mills, Andrew, Davies, Richard H., Worsley, David, 1993. Chem. Soc. Rev. 417–425.
Mozurkewich, Michael, Benson, Sidney W., 1984. J. Phys. Chem. 88 (25), 6429–6435.
Pastrana-Martínez, L.M., Morales-Torres, S., Likodimos, V., Figueiredo, J.L., Faria, J.L., Falaras, P., Silva, A.M.T., 2012. Appl. Catal. B Environ. 123–124, 241–256.
Shahid, Sammia, Fatima, Urooj, Rasheed, Muhammad Zaheer, Asghar, Muhammad Nadeem, Zamam, Sabah, Sarwar, M.N., 2020. Appl. Nanosci. 10, 187–197.
Sorathiya, Kalpesh, Mishra, Biswajit, Kalarikkal, Abhishek, Reddy, Kasala Prabhakar, Gopinath, S., Khushalani, Deepa, 2016. Nature Scientific Reports 6, 35075.
Stathi, Panagiota, Gournis, Dimitrios, Deligiannakis, Yiannis, 2015. Langmuir 31, 10508–10516.
Strom, Henrik, Sasic, Srdjan, 2015. Procedia Engineering 102, 1563–1572.
Sun, H., Wang, S., 2014. Energy Fuels 28, 22–36.
Tien, Huynh Ngoc, Luan, Van Hoang, Hoa, Le Thuy, Khoa, Nguyen Tri, Hahn, Sung Hong, Chung, Jin Suk, Shin, Eun Woo, Hur, Seung Hyun, 2013. Chem. Eng. J. 229, 126–133.
Turro, Nicholas J., Lehr, Gary F., Butcher Jr., Jared, A., Moss, Robert A., Guo, Wenjeng, 1982. J. Am. Chem. Soc. 104 (6), 1754–1756.
Wang, Dengjun, Saleh, Navid B., Sun, Wenjie, Park, Chang Min, Shen, Chongyang, Aich, Nirupam, Peijnenburg, Willie J.G. M., Zhang, Wei, Jin, Yan, Su, Chunming, 2019. Environ. Sci. Technol. 53 (13), 7265–7287.
Ward, Thomas M., Weber, Jerome B., 1968. J. Agric. Food Chem. 16 (6), 959–961.
Xiao, Kemeng, Wang, Tianqi, Sun, Mingzhe, Hanif, Aamir, Gu, Qinfen, Tian, Bingbing, Jiang, Zhifeng, Wang, Bo, Sun, Hongli, Shang, Jin, Wong, Po Keung, 2020. Environ. Sci. Technol. 54 (1), 537–549.
Xu, Ximeng, Chen, Weiming, Zong, Shaoyan, Ren, Xu, Liu, Dan, 2019. J. Hazard Mater. 377, 62–69.
Yang, Yan, Sun, Mengying, Zhou, Jin, Mac, Jianfeng, Komarneni, Sridhar, 2020. Chemosphere 244, 125588.
Yu, Jiaguo, Yu, Xiaoxiao, 2008. Environ. Sci. Technol. 42 (13), 4902–4907.
Zhang, Lixin, Li, Na, Jiu, Hongfang, Qi, Guisheng, Huang, Yunjie, 2015. Ceram. Int. 41, 6256–6262.
Zheng, Y., Liu, J., Liang, J., Jaroniec, M., Qiao, S.Z., 2012. Energy Environ. Sci. 5, 6717–6731.